

RSC Advances

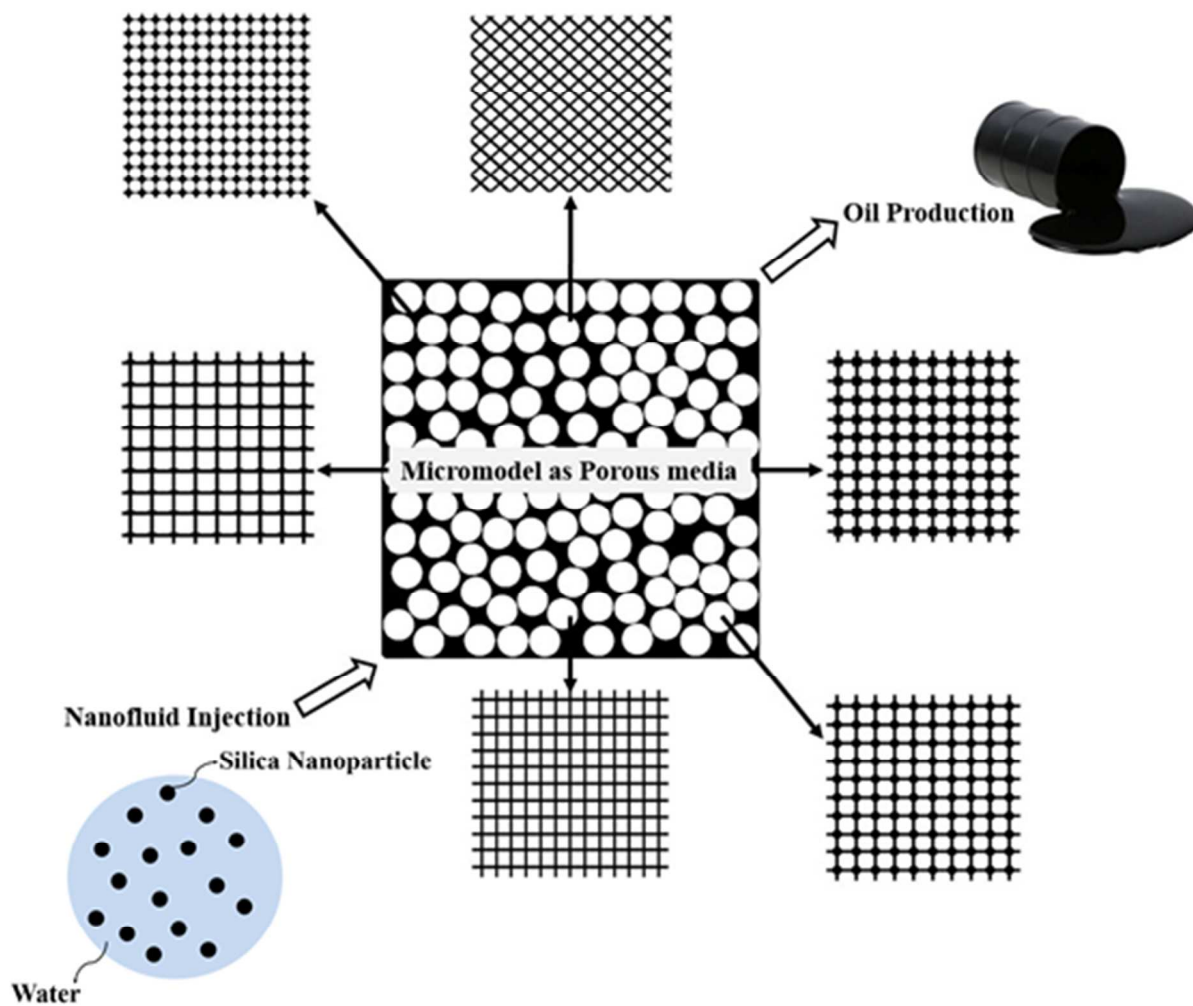


This is an *Accepted Manuscript*, which has been through the Royal Society of Chemistry peer review process and has been accepted for publication.

Accepted Manuscripts are published online shortly after acceptance, before technical editing, formatting and proof reading. Using this free service, authors can make their results available to the community, in citable form, before we publish the edited article. This *Accepted Manuscript* will be replaced by the edited, formatted and paginated article as soon as this is available.

You can find more information about *Accepted Manuscripts* in the [Information for Authors](#).

Please note that technical editing may introduce minor changes to the text and/or graphics, which may alter content. The journal's standard [Terms & Conditions](#) and the [Ethical guidelines](#) still apply. In no event shall the Royal Society of Chemistry be held responsible for any errors or omissions in this *Accepted Manuscript* or any consequences arising from the use of any information it contains.



Application of CFD to Evaluate Pore Morphology Effect in the Nanofluid Flooding for Enhanced Oil Recovery

Reza Gharibshahi^a, Arezou Jafari^{a,*1}, Ali Haghtalab^a, Mohammad Saber Karambeigi^b

^aChemical Engineering Department, Tarbiat Modares University, Tehran, Iran

^bTOR/EOR Research Institute, Tehran, Iran

Abstract

In this study a computational fluid dynamics (CFD) method has been developed to simulate the effect of pore morphology and its distribution in a 2D micromodel on the enhanced oil recovery factor in the nanofluid flooding. Seven types of micromodels with different schematic and pore shape were considered. SiO_2 nanoparticles, dispersed in the distilled water, were used for preparation of the nanofluid and flooding operation. To generate the desirable porous media, the geometry of micromodels was generated using the commercial grid generation tool, Gambit 2.3. Then, the momentum and mass transport equations were solved based on the finite volume method using the Fluent 6.3 software to investigate the displacement of oil at the pore scale. In order to better understand nanoparticles effects and to confirm the validity of CFD simulations, numerical results have been compared with the experimental data. Some parameters influence such as heterogeneity of pores, connectivity of pores with or without throat line, tortuosity and pore shape on the enhanced oil recovery, breakthrough time and fluid trapping in the porous media was investigated. From the results, it has been found that random generation of pore distribution illustrates better results compared to the homogeneous pore distribution. In addition, in the presence of nanoparticles in the injected fluid the number of fingers decreases. The fingering effect has a main effect on the oil recovery factor and less fingering effect have more recovery factor. So, in the homogeneous pattern the nanofluid flow in the porous media is uniform and symmetric. But in the random distribution model, the fluid flow is more realistic and similar to the fluid flow in reservoirs.

Keyword: Pore Morphology, Nanofluid Flooding, Micromodel, EOR, CFD, Throat Line.

¹Corresponding author E-mail: ajafari@modares.ac.ir
Tel.: +98 2182884982

1. Introduction

There is a burgeoning tendency toward application of new technologies in the enhanced oil recovery (EOR) processes by which the oil production can be improved substantially. Nanotechnology which is the science of materials at nano-scale, offers outstanding performances in this way and it can establish an effective bridge between large scale and atomic as well as molecular scales. The unique characteristics of nanoparticles such as mechanical, chemical and thermal properties are significant driving forces for their applications in various EOR methods.¹

Generally EOR technologies divided into several main categories; namely miscible/immiscible methods, chemical processes, as well as thermal techniques.^{2, 3} The conventional EOR approaches would suffer from different demerits; for instance, low sweep efficiency in heterogeneous porous media, instability in unconventional reservoirs, economic infeasibility, possibility of formation damage e.g. permeability reduction, drastic consequences for the environment, and corrosion potential. By contrast, addition of nanoparticles due to their nano-size can solve several drawbacks regarding conventional methods and increase the sweep efficiency of the displacing fluid. Because nanoparticles improve the interfacial properties and also thermal conductivity of the base fluids. In addition, they are stable in high temperature/pressure conditions, environmentally compatible, and cost-effective.^{1, 4} It is worthy to mention that almost all EOR methods are expensive processes, but myriad advantages of the nanofluid flooding can compensate its economic drawbacks.

Therefore, among available products applied in different EOR methods, nanofluids (nanoparticles suspended in a fluid) have vital importance.^{5, 6} Addition of nanoparticles can optimize the properties of displacing fluids such as density, viscosity, interfacial tension between oil and water, thermal conductivity and specific heat.^{7, 8} In practical thought, nanofluid flooding improves the macroscopic sweep efficiency through reduction of the fingering effect. Therefore, oil of unswept zones can be recovered.^{9, 10} Also it can affect the microscopic displacement efficiency via reduction of interfacial tension^{11, 12} and change the wettability of the reservoir rock from oil-wet to water-wet.^{4, 7, 13, 14} Moreover, nanofluids reduce the viscosity of heavy oil,^{11, 12} and experimental data confirmed that the nanofluid flooding compare to water flooding increases the oil recovery factor.¹⁴ Because of huge advantages of nanofluids it seems that in the near future nanofluids flooding can be applied instead of usual EOR methods in the field scale.

So it is serious to investigate about effective factors that have influence in the nanofluid flooding. An important parameter for the effective increase of recovery factor is type of the base fluid which disperses nanoparticles⁴. Furthermore, selection of a suitable nanoparticle is another vital variable. Several types of nanoparticles such as SiO_2 , TiO_2 , CuO and Al_2O_3 are reported in the literature for EOR applications.¹⁵

Since all the researches that have been performed about the nanofluid flooding are experimental work, for the fast promotion of this high-potential technique simulations and modeling studies can help researchers. Therefore, in this work, computational fluid dynamics (CFD) approach is utilized for this purpose¹⁶ that has not been reported yet in the literature. CFD technique is used for analyzing the systems involve fluid flow, heat transfer and associated phenomena such as chemical reactions by means of computer-based simulation.¹⁷⁻¹⁹ This technique is very powerful and spans a wide range of industrial and non-industrial application areas. In this method, partial differential equations are solved numerically through their conversion into algebraic equations.^{20, 21} Among available approaches, finite volume method is more applicable, especially for incompressible flows.

The advantages of CFD compared to the laboratory methods are the ability of studying special and critical conditions in a process, facilitating design of equipment and reducing time and costs and also obtaining complete information and accurate details of the solution. Therefore, CFD has been used in many gas and oil industries like drilling,²²⁻²⁴ erosion,^{25, 26} separator,²⁷ subsea equipment,²⁸ EOR²⁹ and many other fields. However, studying the effects of pore morphology and pores distribution in the nanofluid flooding by a CFD technique has not been carried out yet.

In order to study the pore morphology, a porous medium is required. Micromodels as two dimensional porous media are defined as microscale apparatuses that enable visual observation of phase displacement behavior at the pore level. They are good alternatives for sand packs and cores because a major limitation of studies implemented in such media are their black-box features.³⁰ The materials available for fabrication of micromodels are glass, silicon or polymers like polydimethylsiloxane (PDMS). Another priority for the application of micromodels is possibility of designing, fabricating and studying selective patterns.³¹ For this purpose, patterns can be categorized into innovative (designed based on the geometry required for a special study) patterns such as simple pore networks of circular,³² triangular,³³ quadratic³⁴ or reservoir prototype patterns by taking SEM images from the thin section of reservoir rocks.²⁹

It is worthy to mention that different processes and parameters can be evaluated in porous media using micromodels such as oil recovery factor,^{35, 36} breakthrough time,³⁷ viscosity reduction,⁷ changes of the interfacial surface tension,^{38, 39} wettability alteration,^{40, 41} miscible or immiscible injections,^{42, 43} mass transfer,^{44, 45} chemical reactions,^{46, 47} capillary pressure⁴⁸ and heterogeneity.⁴⁹

Previous investigations indicate that pattern characteristics of micromodels are important for precise studies in the pore-scale experiments; for example, pore morphology, coordination number, pore shape and the location of pore-necks on the pore-body.³³ Emami Meybodi *et al.*³³ evaluated the effect of pore morphology and wettability on the microscopic and macroscopic displacement efficiencies in polymer flooding. They concluded that the random network with triangular pore shape shows better results than other patterns. Dehghan *et al.*⁵⁰ carried out experimental work to understand the role of pore geometry and connate water on miscible

displacement of heavy oil with different hydrocarbon solvents in five-spot micromodels. They found that the displacement efficiency is improved more in patterns with higher coordination number and lower pore-throat size. Moreover, heterogeneity of the porous media reduces the miscible displacement efficiency. Mason and Morrow⁵¹ as well as Princen⁵² showed that angular cross-section pores have many qualitative features represented by real porous media and there is identical capillary behavior in a tube having the same shape factor even though they are geometrically different.

As the pore morphology of micromodels has a considerable effect on fluids displacement and there is no study about the pore shape in the nanofluid flooding; in this work, the effect of different micromodel characteristics on the performance of nanofluid flooding is evaluated using CFD modeling for the first time. In other words, the objective of current work is simulating the effect of pore morphology and distribution in terms of pore-throat connectivity, heterogeneity, pore shape, pore-throat connectivity and tortuosity of pores in the porous media on different responses such as oil recovery factor, trapping effect, and mobility control (breakthrough time) that has not been discussed in any publication yet. The laboratory data required for validation of simulation results is prepared through pore-scale microvisual experiments in glass micromodels.¹⁴

2. Numerical implementation

2.1. Geometry creation

Geometry of porous media was created using Gambit 2.3 (Fluent Inc.). Seven patterns of micromodels were produced in which they had the equal size $6 \times 6 \text{ cm}^2$ and porosity $33 \pm 2 \%$ (Fig. 1). Moreover, the physical properties of patterns were selected in which they were representative of the pattern used by Maghzi *et al.*¹⁴ due to the validation of simulation results with their experimental work. The characteristics of the designed patterns are shown in Table 1. The random distribution of model A was prepared by programming developed in Matlab and C++ in a way to keep the porosity constant (33 %). Two conditions were considered to spread the circles. The former was existence of circles in the square and the latter was lack of contact between circles. Then to make the porous media, circles surface area was subtracted from the square.

To divide micromodels (A-G) into discrete control volumes, about 2.5×10^5 , 5.5×10^5 , 3.4×10^5 , 3.6×10^5 , 2.9×10^5 , 3.4×10^5 and 3.3×10^5 computational cells were used, respectively. It should be mentioned that inlet and outlet ports had larger mesh size than other sides due to the more accuracy required for the calculations at inlet and outlet ports. Tri/pave mesh was chosen for the faces because this type is better for meshing and linking the curved edges of a circle with angled surface of the micromodels.

2.2. Grid independency

For investigating the grid independency, various types of grids with different mesh size were generated. Then for each grid the governing equations were solved for water flow rate 8×10^{-4} cc/min and $\Delta t = 0.1$ s. It should be mentioned that several tests with different time intervals (0.01, 0.1 and 1 s) were done to examine the effect of time step on results accuracy. Finally it was obtained that for micromodels the difference was negligible. Therefore, to save time and computational cost $\Delta t = 0.1$ s was used for simulations, and simulations continued until the steady state condition was achieved.

The fluid Pressure drops in porous media were considered to compare grids. To do this, total pressure at the inlet and outlet were calculated and then equation (1) was used to estimate the percent of relative error.

$$Error = \frac{|\Delta P_1 - \Delta P_2|}{\Delta P_1} \times 100 \quad (1)$$

Where ΔP_1 is the pressure difference between the inlet and outlet with finer mesh and ΔP_2 is the pressure difference in coarser mesh. Table 2 shows the mesh size, number of cells and nodes that produce in any grid, the pressure drop between inlet and outlet and the value of error for each micromodel. When the relative error between two consecutive grids was calculated as low in which it can be neglected, the large size grid was selected as the main grid. As a result, the selected grids of micromodels A to G had 136449, 343979, 194980, 208534, 181371, 261329 and 204572 nodes, respectively. Selecting the final grid with larger mesh size and fewer node (cell) numbers for flooding can help to reduce computation calculations. As an example, the grid of model A is depicted in Fig. 2.

Velocity inlet and pressure outlet were used as boundary conditions for inlet and outlet ports, respectively. Velocity inlet boundary conditions are used to define the flow velocity along with all relevant scalar properties of the flow at inlets. Then, for allowing the nanofluid to exit from the model via a 5 spot pattern, the pressure outlet was selected for outlet port. No flow is entering into or exiting from other edges and so wall boundary conditions were assumed.

2.3. Governing equations

Mixture model as a simplified multiphase model was used to solve the equations. Moreover, liquid-solid flows can be modeled using this method. Mixture method can model n phases through solving the momentum, continuity and energy equations for the mixture⁵³ and the volume fraction equations for the secondary phases and algebraic expressions for the relative velocities. The relevant equations are as follows:⁵⁴

Conservation of mass:

$$\frac{\partial}{\partial t}(\rho_m) + \nabla \cdot (\rho_m \vec{V}_m) = 0 \quad (2)$$

Conservation of momentum:

$$\frac{\partial}{\partial t}(\rho_m \vec{v}_m) + \nabla \cdot (\rho_m \vec{v}_m \vec{v}_m) = -\nabla P_m + \nabla \cdot (\mu_m \nabla \vec{V}_m) + \nabla \cdot \left(\sum_{k=1}^n \varphi_k \rho_k \vec{V}_{dr,k} \vec{V}_{dr,k} \right) \quad (3)$$

Where the mixture velocity, density and viscosity sequentially are as follows:

$$\vec{V}_m = \frac{\sum_{k=1}^n \varphi_k \rho_k \vec{V}_k}{\rho_m} \quad (4)$$

$$\rho_m = \sum_{k=1}^n \varphi_k \rho_k \quad (5)$$

$$\mu_m = \sum_{k=1}^n \varphi_k \mu_k \quad (6)$$

The drift velocity of kth phase is:

$$\vec{V}_{dr,k} = \vec{V}_k - \vec{V}_m \quad (7)$$

The volume fraction equation for the secondary phase (p) can be obtained:

$$\frac{\partial}{\partial t}(\varphi_p \rho_p) + \nabla \cdot (\varphi_p \rho_p \vec{V}_m) = -\nabla \cdot (\varphi_p \rho_p \vec{V}_{dr,p}) \quad (8)$$

The slip velocity (relative velocity) is defined as the velocity of a secondary phase (p) relative to the velocity of the primary phase (f):

$$\vec{V}_{pf} = \vec{V}_p - \vec{V}_f \quad (9)$$

The drift velocity is related to the relative velocity as:

$$\vec{V}_{dr,p} = \vec{V}_{pf} - \sum_{k=1}^n \frac{\varphi_k \rho_k}{\rho_{eff}} \vec{V}_{fk} \quad (10)$$

Selecting appropriate values of the under-relaxation factors guarantees a reasonable rate of convergence. The under-relaxation factors were assigned as 0.3 for pressure, 1 for density and body forces, 0.7 for momentum, 0.1 for slip velocity and finally 0.2 for volume fraction. If the normalized residuals became smaller than 0.001, then equations of mass and momentum would be satisfied to achieve convergence. The maximum residual value occurs after the first few iterations when the normalization factors used for the mass and momentum. Using the mixture model to solve the problem, these assumptions were taken:

- 1- Two phase flow condition.
- 2- Primary phase is oil and the secondary phase is water and nanofluid in the validation and other tests, respectively.
- 3- Initial water saturation is zero ($S_{wi}=0$) and the water injected into the micromodel is distilled water.
- 4- Unsteady state condition.
- 5- All experiments were carried out at ambient temperature and pressure.
- 6- The flow rate is constant as 8×10^{-4} cc/min during flooding.
- 7- $\Delta t=0.1$ s has been selected for all simulations.
- 8- To establish a good comparison between all the models, iterations were continued until the rate of oil production remained constant. So all flooding operations stopped at 10000 s (or 1 PV of the injected fluid) after injection of the nanofluid.

3. Results and discussion

3.1. Nanofluid flooding

As available publications,⁵⁵⁻⁵⁸ confirm that silica nanoparticles have high potential to enhance the oil recovery factor, in this study the selected nanofluid consist of 4 wt% SiO_2 nanoparticle (Table 3) in distilled water. It is assumed that silica nanoparticles are spherical and in order to avoid aggregation of nanoparticles, the particles volume fraction and diameter have been selected small enough. The nanofluid properties were calculated according to equation (11) and (12):⁵⁹

$$\rho_{nf} = \varphi \times \rho_p + (1 - \varphi) \times \rho_{bf} \quad (11)$$

$$\mu_{nf} = \mu_{bf} \times \left(1 - \frac{\varphi}{\varphi_m}\right)^{-\eta \varphi_m} \quad (12)$$

Where ρ_{nf} and ρ_{bf} are densities of nanofluid and the base fluid, μ_{nf} and μ_{bf} shows nanofluid and the base fluid viscosity, respectively. φ represents the nanoparticles volume fraction, $\varphi_m = 0.5$ and $\eta = 2.5$.⁵⁹ It should be mentioned that φ_m , the maximum particles volume fraction varies from 0.495 to 0.54 under quiescent conditions, and is approximately 0.605 at high shear rates. But because in this study the shear rate is not high, this parameter assumed as 0.5.

In simulations it is assumed that firstly micromodels are saturated with the crude oil and properties of the oil is the same as Azadegan heavy oil field located in the south west of Iran (Table 4).

3.2. The heterogeneity effect

The geometry of reservoir rocks is complex because it consists of the pores with different size and random distribution as well as lots of dead end pores. Modeling of two phase flow in such

media is very complicated. Therefore, researchers try to facilitate the characteristics of patterns representing of reservoirs porous media.⁶⁰ In this section, the effect of pore heterogeneity was investigated in micromodel A. As Results are illustrated in Fig. 3, the fluid flow in this model is relatively similar to that in rock reservoir. Moreover, the amount of oil recovery factor in nanofluid flooding is in good agreement with the experimental data (relative error is 5.17%). In other words, the prediction of this model compare to other patterns for the oil recovery factor in the nanofluid flooding is more accurate. As the nanofluid volume fraction contours shown in Fig. 4, the fluid flow pattern is the nearest one to the typical flow of two phase flow in real porous media. Because fingering and trapping effects of the injected front can be observed approximately well. It should be considered that if the research focus is on trapping effect, it cannot be investigated thoroughly in model A.

3.3. The effect of connecting pores with/without throat lines

Patterns with different geometry and physical properties can be designed to be representative of a specific porous model. Among different properties, the pore to throat connectivity may be determinative to study parameters affecting the nanofluid flow and oil displacement in porous media.

In this section models B and C were designed to study the effect of pores connectivity in which pores in model B were not connected through throats while model C were connected. Results showed that this factor can cause the oil recovery in which the pattern having pores connected with the throat lines (model C) produces more oil and has higher relative error compared to the experimental data (Fig. 5). It is worthy to mention that the experimental porous shape is representative of a real reservoir, in that case the pattern of Maghzi *et al.*¹⁴ has been chosen for comparison of numerical results.

The nanofluid volume fraction contours of models B and Care depicted in Fig. 6. It can be found that the nanofluid flow is symmetric in both models. The front progress in the model C is more uniform (piston-like) than model B which injected front has obviously been fingered. On the other hand, the macroscopic sweep efficiency is higher in model C.

3.4. The effect of pore shape

The effect of pore shape on the oil recovery factor in micromodels was investigated in this section. Two scenarios were considered for studying the effect of pore shape: with and without the throat line. In the first scenario, three types of micromodels with different pore shapes were selected as circular (model C), quadratic (model D) and triangular (model E). Numerical results indicate that the oil recovery factor in the model with quadratic pore shape has the most precise prediction of experimental data, because its relative error was the least as shown in Fig. 7. The nanofluid volume fraction contours of these three models have been presented in Fig. 8. It can be

seen that in model E, compared to models C and D, the higher surface is in contact with the nanofluid and more fingers occur in this model.

The second scenario was run for models without throat line connections. For this purpose, two micromodels with different pore shapes as circular (model B) and quadratic (model F) were considered. Fig. 9 shows the oil recovery factor resulted from simulation runs and reveals that model B has more precise prediction compared with model F. But as Fig. 10 illustrates, the fluid flows in both models are very similar although model B has lower relative error.

3.5. Pores tortuosity effect

The angle between the fluid flow direction in porous media and pores is an important parameter for investigation of the oil recovery factor in the micromodel flooding operations.⁶¹ If the fluid flow direction is the same as the direction of connections between the pores or pore-throat line in a model, the nanofluid can move easily in the model through the lines. Therefore, the oil recovery factor is low because the mobility of injected front is very high in such models and prediction of the EOR behavior is not correct.

For investigating the pore tortuosity effect, models F and G were designed and studied. Model F has predicted the experimental data better than model G (Fig. 11). Fig. 12 shows the nanofluid volume fraction contours in model F and G, respectively. The Front injection in model G because of less tortuosity has rapid breakthrough. That is due to the high mobility of the injected fluid in such media. But in model F the residence time of the injected fluid is more and front of the injected fluid could invade to other zones. In that case the macroscopic sweep efficiency is higher in model F.

3.6. The effect of micromodel type on the oil recovery factor

The nanofluid flooding in models A-G is performed and the relative errors between numerical results and experimental data for the oil recovery factor have been determined and tabulated in Table 5. This Table and also previous results obviously indicate that the geometry of micromodel patterns has a determinative factor in which it influences the results of oil recovery factor. In other words, in simulations with constant properties of oil and displacement fluids, micromodels show different oil recovery factors although they approximately have the same dimensions and porosities.

Model A with random distribution of pores has the best results with 5.17% relative error. By comparing the relative error between models with and without throat line, it has been found that connection type of pores can affect the oil recovery factor. So it is better to remove the connections of pores with a specified line and allow the injected fluid to move freely in porous

media and chooses the own pathway based on the physical properties of model and not according to the path that we have chosen for it.

3.7. Effect of the breakthrough time

The effect of pattern type on the breakthrough time of displacing fluid containing nanoparticles was studied at constant injection rate 8×10^{-4} cc/min. As shown in Fig. 13, it can be found that models C and G have the longest (6742 s) and fastest (2519 s) breakthrough time, respectively. Because in model C, the pore necks are small and the fluid flow in this micromodel is very difficult. Therefore, the flow goes around to the corners and two sides of the model and it takes more time to make breakthrough, but the pore morphology of model G is not complex and the connection with the pores are simple and the pore necks have enough size to pass the fluid flow easily. Hence, the breakthrough time in model G is faster than other models. The oil recovery factors at breakthrough time and the ultimate oil recoveries have been shown in Fig. 14. It can be observed that this difference is 20.14% for model A which is larger than other models while model D has the smallest difference as 4.34%.

3.8. Trapping effect

Oil and gas of hydrocarbon reservoirs may be trapped in porous media which is known as trapping effect. The mechanism of this phenomenon is not understood well, so the mathematical equations cannot define this complex function perfectly. The fluid trapping, however, depends on different factors such as the porous medium pore structure, fluid-rock interaction and fluid-fluid interaction.⁶² At the microscopic level of EOR operations, all of original oil in-place cannot be produced and considerable amount of oil remains intact and trapped in porous media. For studying this effect, the magnified volume fraction contours of designed micromodels in the nanofluid flooding were compared in Fig. 15. It can be concluded that models whose pores have corners (e.g. models D and E with quadratic and triangular pore shapes, respectively) are suitable for studying the trapping effect in porous media. In models D and E after the nanofluid flooding some oil remains trapped in the corners of the pore and the injected fluid cannot overcome the capillary pressure of the trapped phase to mobilize it. It should be mentioned that in the Fig. 15 red and blue colors represent the maximum and minimum volume fraction of oil, respectively.

4. Conclusion

In this work, simulation of the nanofluid flooding in various patterns of micromodels having different geometry and pore morphology was lead using computational fluid dynamics. Micromodels contained seven patterns were created with commercial grid generation tool (Gambit 2.3). To investigate the fluid flow in the porous media, the momentum and mass transport equations were solved based on the finite volume method using the Fluent 6.3 software. The effect of some parameters such as heterogeneity, connectivity of the pores with /without

throat lines, pore shape and finally Pores tortuosity effect were studied on the enhanced oil recovery and breakthrough time. The fluid flow in porous media was predicted numerically using the multi-phase model and simulation results were validated with the experimental data. The following results were obtained:

- The fluid flow in models having heterogeneous distribution of pores resembles relatively more to that in the rock reservoir, but the trapping effect cannot investigate perfectly in such models. Results of the oil recovery factor show that the nanofluid flooding in this model has a good agreement with the experimental data.
- The connection between the pores in models decreases the fingering effect and causes the uniform front flow. Therefore, much more area of the porous media will be invaded by the injected fluid and consequently macroscopic sweep efficiency will be increased compared to models without throat line.
- Among models with throat line, those which have quadratic pore shapes have the nearest results and among models without throat line, it can be found that the fluid flow in these models are very similar to each other and are approximately independent from the pore shape. Although the model with circular pore shape have lower relative error than the quadratic pore shape.
- The angle between the direction of fluid flow and pores is an important parameter. The oil recovery factor is lower than experimental results in models that have the same direction of fluid flow and the connection pores. On the other hand, the relative error between numerical results and experimental data in such models are very high.
- Models with random distribution of pores have a good agreement with experimental data with the least relative error 5.17 %. Considering the connection of pores with a throat line increases the oil recovery factor and subsequently the relative error will be raised.
- Models C and G sequentially have the longest and fastest breakthrough time. Also the difference between the ultimate and breakthrough time oil recovery factors in models A and D are larger and smaller, respectively among other models.
- At the microscopic level, models whose pores have corners such as quadratic or triangular pore shapes are suitable for studying the trapping effect in the porous media.

Finally, the results of this study indicate that the model with random distribution of pores (model A) is suitable for future development of simulation studies in nanofluid flooding processes. Recommendations for further studies can be the investigation of nanoparticles impacts on the rock/fluid interactions and properties such as wettability and oil viscosity to thoroughly understand the mechanism of nanofluid transport in porous media and its relevant phenomena in EOR matters.

Acknowledgment

The authors would like to thank Tarbiat Modares University, Iran's National Elites Foundation and Nanotechnology Initiative Council for financial support of this research.

References

1. S. Ponmani, R. Nagarajan and J. Sangwai, *J. Nano Res.*, 2013, **24**, 7-15.
2. S. Lago, H. Rodríguez, M. K. Khoshkbarchi, A. Soto and A. Arce, *RSC Adv.*, 2012, **2**, 9392-9397.
3. A. Muggeridge, A. Cockin, K. Webb, H. Frampton, I. Collins, T. Moulds and P. Salino, *Philos. Trans. R. Soc. A Math. Phys. Eng. Sci.*, 2014, **372**, 20120320.
4. N. Ogolo, O. Olafuyi and M. Onyekonwu, SPE Saudi Arabia Section Technical Symposium and Exhibition, Al-Khobar, Saudi Arabia, 2012.
5. X. Kong and M. Ohadi, Abu Dhabi international petroleum exhibition and conference, Abu Dhabi, UAE, 2010.
6. A. Fletcher and J. Davis, SPE Improved Oil Recovery Symposium, Tulsa, Oklahoma, USA, 2010.
7. Y. Hamed Shokrlu and T. Babadagli, Canadian Unconventional Resources and International Petroleum Conference, Calgary, Alberta, Canada, 2010.
8. A. Roustaei, J. Moghadasi, H. Bagherzadeh and A. Shahrabadi, *Proc. SPE Int. Oilf. Nanotechnol. Conf.*, 2012.
9. M. R. Haroun, S. Alhassan, A. A. Ansari, N. A. M. Al Kindy, N. Abou Sayed, A. Kareem, B. Ali and H. K. Sarma, Abu Dhabi International Petroleum Conference and Exhibition, Abu Dhabi, UAE, 2012.
10. J. Yu, C. An, D. Mo, N. Liu and R. L. Lee, SPE Improved Oil Recovery Symposium, Tulsa, Oklahoma, USA, 2012.
11. L. Hendraningrat and L. Shidong, SPE Russian Oil and Gas Exploration and Production Technical Conference and Exhibition, Moscow, Russia, 2012.
12. T. Skaug, K. Spildo and A. Skaug, SPE Improved Oil Recovery Symposium, Tulsa, Oklahoma, USA, 2010.
13. B. Ju, T. Fan and M. Ma, *China Particuology*, 2006, **4**, 41-46.
14. A. Maghzi, S. Mohammadi, M. H. Ghazanfari, R. Kharrat and M. Masihi, *Exp. Therm. Fluid Sci.*, 2012, **40**, 168-176.
15. B. Suleimanov, F. Ismailov and E. Veliyev, *J. Pet. Sci. Eng.*, 2011, **78**, 431-437.
16. J. Jamali and S. N. Shoghl, *RSC Adv.*, 2014, **4**, 57958-57966.
17. H. Hayer, O. Bakhtiari and T. Mohammadi, *J. Ind. Eng. Chem.*, 2014.
18. S. H. Hosseini, S. Shojae, G. Ahmadi and M. Zivdar, *J. Ind. Eng. Chem.*, 2012, **18**, 1465-1473.
19. J.-B. Ryu, C.-Y. Jung and S.-C. Yi, *J. Ind. Eng. Chem.*, 2013, **19**, 1092-1098.
20. M. Bahiraei, *J. Dispers. Sci. Technol.*, 2013, **35**, 984-996.
21. M. Khan, M. Hussain, Z. Mansourpour, N. Mostoufi, N. Ghasem and E. Abdullah, *J. Ind. Eng. Chem.*, 2014.
22. H. I. Bilgesu, N. Mishra and S. Ameri, Eastern Regional Meeting, Lexington, Kentucky, USA, 2007.
23. M. T. Byrne, M. A. Jimenez, E. A. Rojas and E. Castillo, SPE European Formation Damage Conference, Noordwijk, The Netherlands, 2011.
24. A. I. Mohammed, G. Oluyemi and S. D. Ibrahim, SPE Nigeria Annual International Conference and Exhibition, Lagos, Nigeria, 2013.
25. A. Farahani, M. Lastiwka, D. C. Langer, B. Demirdal, C. M. Matthews, J. Jensen and A. Reilly, SPE Annual Technical Conference and Exhibition, Texas, USA, 2011.
26. R. Russell and E. Marsis, SPE Heavy Oil Conference-Canada, Calgary, Alberta, Canada, 2013.
27. N. Kharoua, L. Khezzar and H. N. Saadawi, Abu Dhabi International Petroleum Conference and Exhibition, Abu Dhabi, UAE, 2012.
28. Y. Lu, M. Agrawal and H. B. Skeels, Offshore Technology Conference, Texas, USA, 2011.
29. T. Clemens, K. Tsikouris, M. Buchgraber, L. M. Castanier and A. Kovscek, *SPE Res. Evalu. & Eng.*, 2013, **16**, 144-154.
30. S. Mohammadi, A. Maghzi, M. Ghazanfari, M. Masihi, A. Mohebbi and R. Kharrat, *Energy sources*, 2013, **35**, 193-201.
31. C. Tsakiroglou and D. Avraam, *J. Mater. Sci.*, 2002, **37**, 353-363.
32. M. Robin, J. Behot and V. Sygouni, SPE Improved Oil Recovery Symposium, Tulsa, Oklahoma, USA, 2012.
33. H. Emami Meybodi, R. Kharrat and M. Nasehi Araghi, *J. Pet. Sci. Eng.*, 2011, **78**, 347-363.
34. S. Mohammadi, M. Hossein Ghazanfari and M. Masihi, *J. Pet. Sci. Eng.*, 2013, **110**, 40-54.
35. S. Mei, J. L. Bryan and A. Kantzas, SPE Heavy Oil Conference Canada, Calgary, Alberta, Canada, 2012.
36. M. Sohrabi, G. Henderson, D. Tehrani and A. Danesh, SPE Annual Technical Conference and Exhibition, Texas, USA, 2000.
37. P. Bedrikovetsky, *Transp. porous media*, 2008, **75**, 335-369.
38. A. Mandal, A. Bera, K. Ojha and T. Kumar, SPE International Oilfield Nanotechnology Conference and Exhibition, Noordwijk, The Netherlands, 2012.
39. F. Qiu, Canadian Unconventional Resources and International Petroleum Conference, Calgary, Alberta, Canada, 2010.
40. C. Chalbaud, M. Robin, S. Bekri and P. Egermann, International symposium of the society of core analysts, Calgary, Canada, 2007.
41. C. Laroche, O. Vizika and F. Kalaydjian, *Pet. Geosci.*, 1999, **5**, 65-69.
42. A. Danesh, D. Krinis, G. Henderson and J. Peden, *J. Pet. Sci. Eng.*, 1989, **2**, 167-177.
43. C. Zhang, M. Oostrom, T. W. Wietsma, J. W. Grate and M. G. Warner, *Energy & Fuels*, 2011, **25**, 3493-3505.
44. C. A. Kennedy and W. C. Lennox, *J. Contam. Hydrol.*, 1997, **24**, 221-246.

45. N. Sahloul, M. Ioannidis and I. Chatzis, *Adv. Water Resour.*, 2002, **25**, 33-49.
46. Y. Kim, J. Wan, T. J. Kneafsey and T. K. Tokunaga, *Environ. Sci. Technol.*, 2012, **46**, 4228-4235.
47. T. W. Willingham, C. J. Werth and A. J. Valocchi, *Environ. Sci. Technol.*, 2008, **42**, 3185-3193.
48. M. H. Ghazanfari, D. Rashtchian, R. Kharrat and S. Vossoughi, *Chem. Eng. Technol.*, 2007, **30**, 862-869.
49. H. Emami Meybodi, R. Kharrat and M. H. Ghazanfari, Europec/EAGE Conference and Exhibition, Rome, Italy, 2008.
50. A. Dehghan, S. Farzaneh, R. Kharrat and M. Ghazanfari, Canadian International Petroleum Conference, Calgary, Alberta, 2009.
51. G. Mason and N. R. Morrow, *J. Colloid Interface Sci.*, 1991, **141**, 262-274.
52. H. Princen, *Colloids and surfaces*, 1992, **65**, 221-230.
53. A. Jafari, *CFD simulation of complex phenomena containing suspensions and flow through porous media*, Lappeenranta University of Technology, 2008.
54. A. Jafari, P. Zamankhan, S. Mousavi and K. Pietarinen, *Chem. Eng. J.*, 2008, **144**, 476-482.
55. L. Hendraningrat and O. Torsæter, *Energy & Fuels*, 2014, **28**, 6228-6241.
56. C. R. Miranda, L. S. De Lara and B. C. Tonetto, Proceedings of the SPE International Oilfield Nanotechnology Conference, Noordwijk, Netherlands, 2012.
57. O. Torsater, B. Engeset, L. Hendraningrat and S. Suwarno, SPE Kuwait International Petroleum Conference and Exhibition, Kuwait City, Kuwait, 2012.
58. A. J. Worthen, H. G. Bagaria, Y. Chen, S. L. Bryant, C. Huh and K. P. Johnston, *J. Colloid Interface Sci.*, 2013, **391**, 142-151.
59. I. Mahbubul, R. Saidur and M. Amalina, *Int. J. Heat Mass Transf.*, 2012, **55**, 874-885.
60. K. Vafai, *Handbook of porous media*, Crc Press, New York, 2nd edn., ch. 4, p.144,2010.
61. J. Cai and B. Yu, *Transp. porous media*, 2011, **89**, 251-263.
62. M. Sahimi, *Flow and transport in porous media and fractured rock: from classical methods to modern approaches*, John Wiley & Sons, Weinheim, Germany, 2nd rev., ch. 14, p. 539,2012.

Nomenclature

S_{wi}	Initial water saturation
$\vec{V}_{dr,k}$	Drift velocity of k th phase
$\vec{V}_{dr,p}$	Drift velocity of a secondary phase
\vec{V}_f	Velocity of the primary phase
V_k	Velocity of k th phase
\vec{V}_m	Mixture velocity
\vec{V}_p	Velocity of a secondary phase
\vec{V}_{pf}	Slip velocity

Greek letters

ΔP_1	Pressure difference between the inlet and outlet with finer mesh
ΔP_2	Pressure difference between the inlet and outlet with coarser mesh
Δt	Time step
μ_{bf}	Viscosity of base fluid
μ_m	Mixture viscosity
μ_{nf}	Viscosity of nanofluid
μ_p	Viscosity of a secondary phase
ρ_{bf}	Density of base fluid

ρ_m	Mixture density
ρ_{nf}	Density of nanofluid
ρ_p	Density of a secondary phase
ϕ	Volume fraction of nanoparticles
ϕ_p	Volume fraction of a secondary phase

Subscripts

bf	Base fluid
dr	Drift
F	Primary phase
K	k th phase
M	Mixture
nf	Nanofluid
p	Secondary phase

List of Figures

Fig. 1. The schematic geometry of designed patterns; (a) overall appearance with location of inlet and outlet ports (b-g) other patterns, for better visualization they have been magnified.

Fig. 2. (a) Model A, (b) a close-up window of model A for better visualization.

Fig. 3. The heterogeneity effect on the oil recovery factor (model A).

Fig. 4. The nanofluid volume fraction contour in model A.

Fig. 5. The effect of pore connectivity on the oil recovery factor. Models B and C are without and with the throat, respectively.

Fig. 6. Volume fraction contours of the nanofluid in models B and C.

Fig. 7. The oil recovery factor of models C, D and E with different pore shapes.

Fig. 8. The nanofluid Volume fraction contours in models C, D and E.

Fig. 9. The oil recovery factor of models without throat connections.

Fig. 10. The nanofluid volume fraction contours in models B and F.

Fig. 11. The effect of angle between fluid flow direction and pores connection on the oil recovery factor.

Fig. 12. The nanofluid volume fraction contours in model F and G.

Fig. 13. The nanofluid breakthrough time in different micromodels.

Fig. 14. The oil recovery factor at breakthrough time and the ultimate oil recovery.

Fig. 15. Nanofluid volume fraction contours in models A-G at the pore scale level.

Fig. 1.

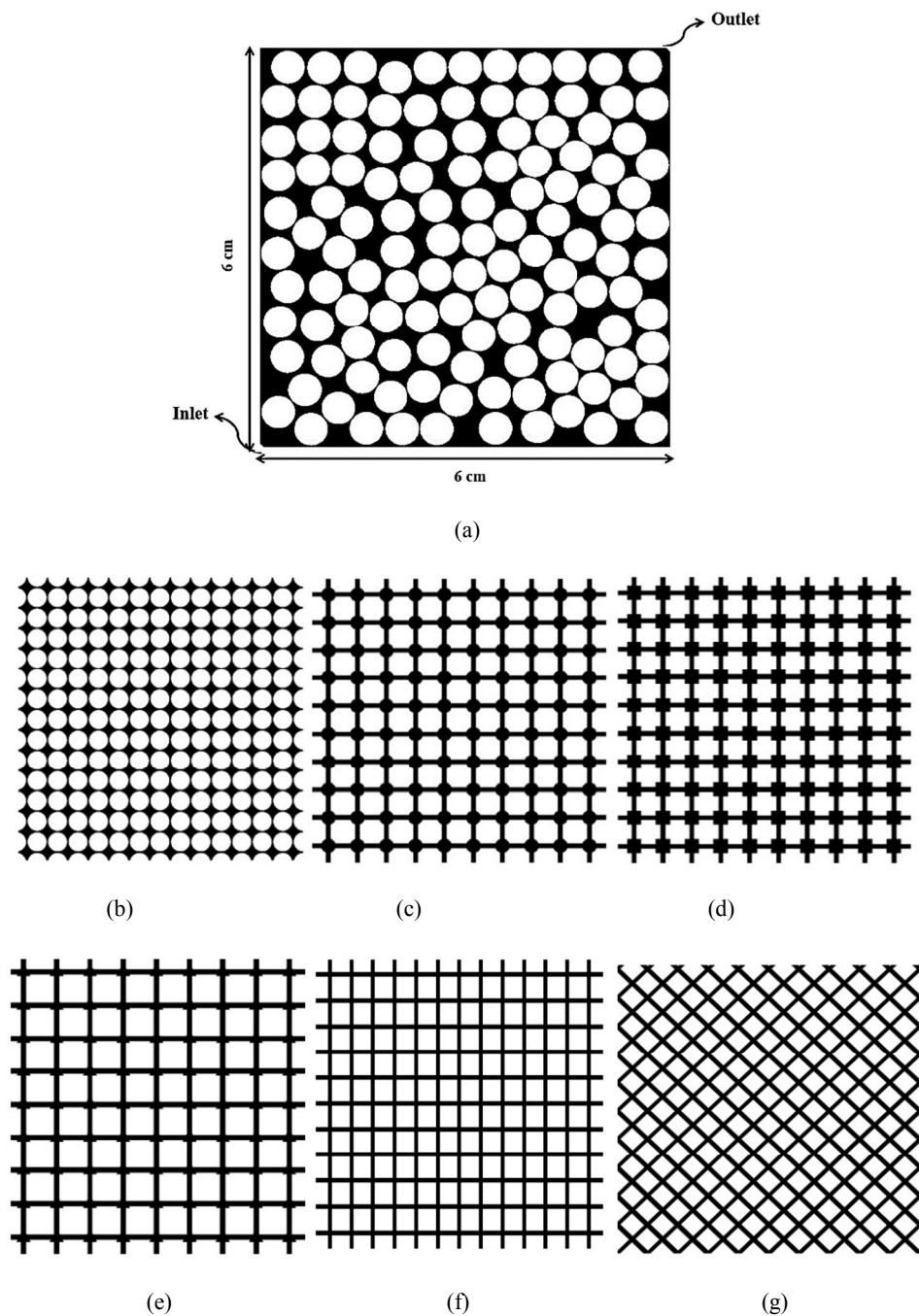


Fig. 1. The schematic geometry of designed patterns; (a) overall appearance with location of inlet and outlet ports (b-g) other patterns, for better visualization they have been magnified.

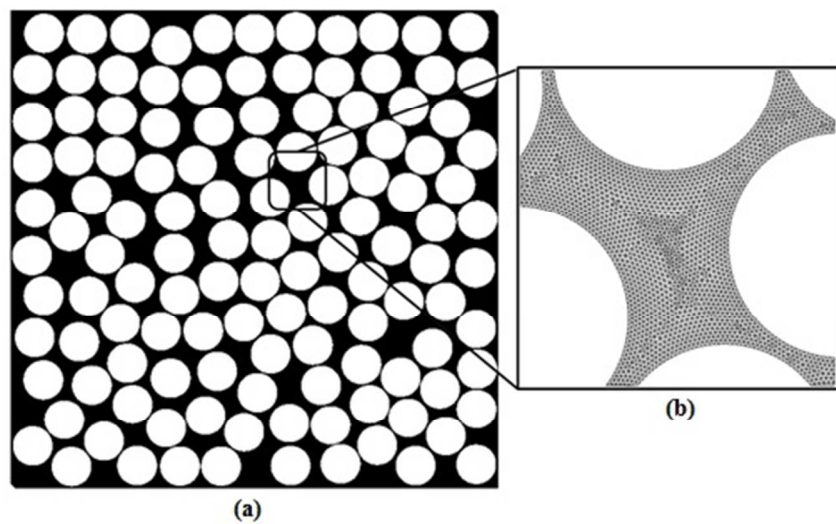
Fig. 2.

Fig. 2. (a) Model A, (b) a close-up window of model A for better visualization.

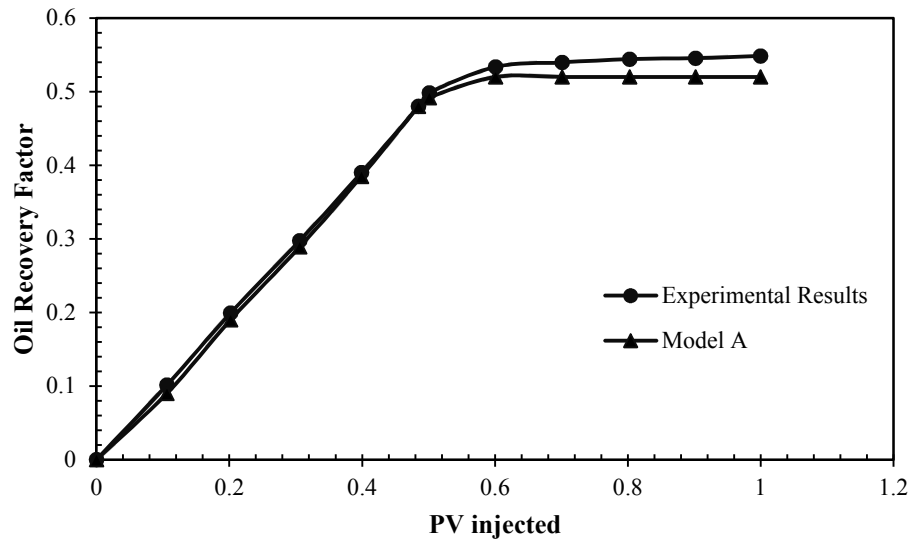
Fig. 3.*Fig. 3.* The heterogeneity effect on the oil recovery factor (model A).

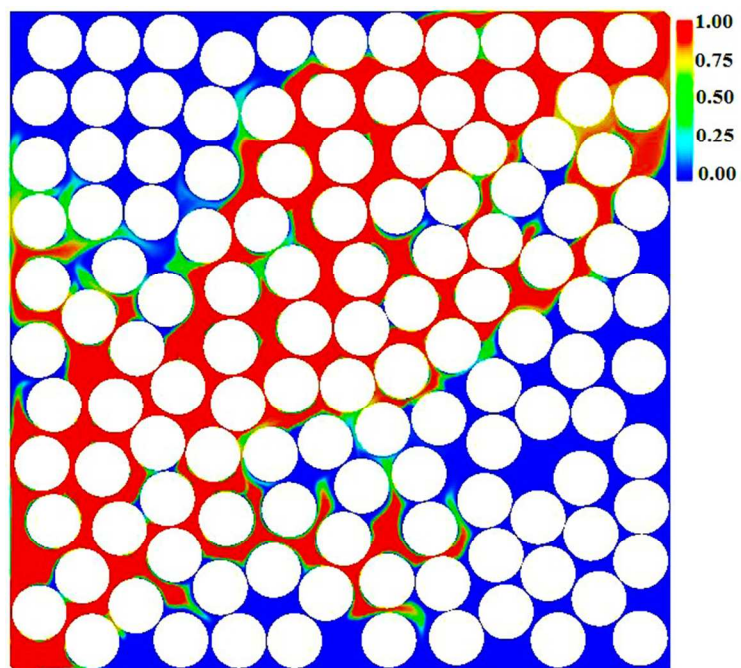
Fig. 4.*Fig. 4.* The nanofluid volume fraction contour in model A.

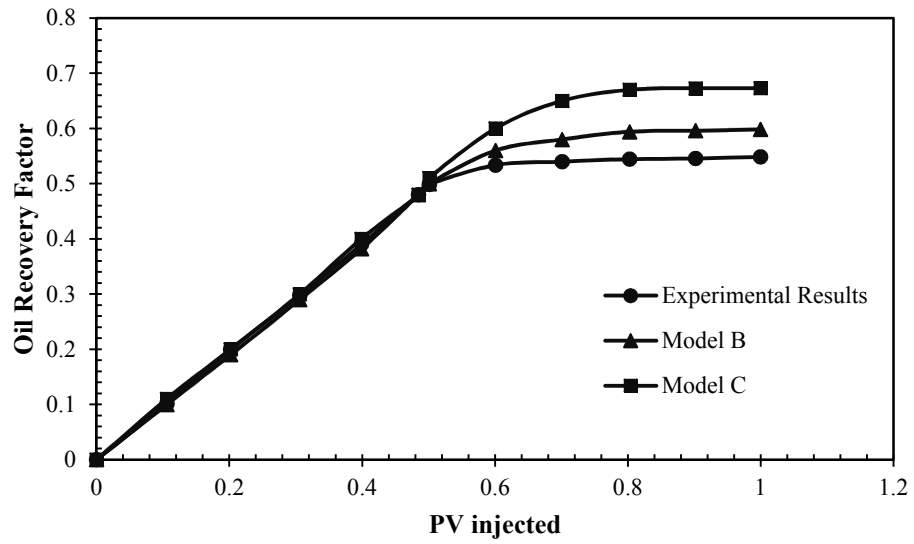
Fig. 5.

Fig. 5. The effect of pore connectivity on the oil recovery factor. Models B and C are without and with the throat, respectively.

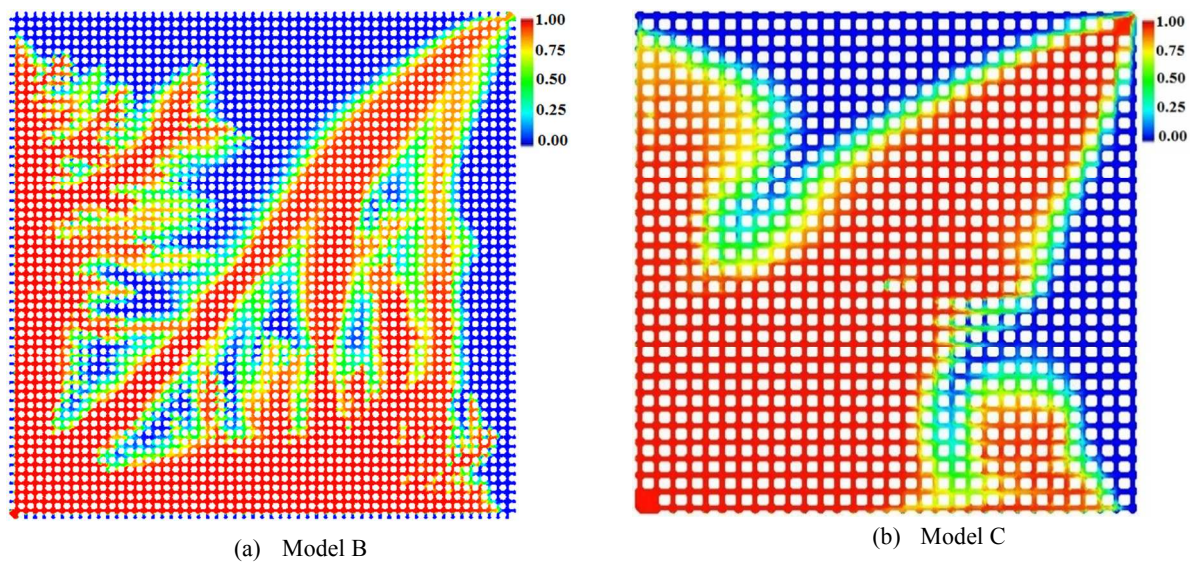
Fig. 6.*Fig. 6.* Volume fraction contours of the nanofluid in models B and C.

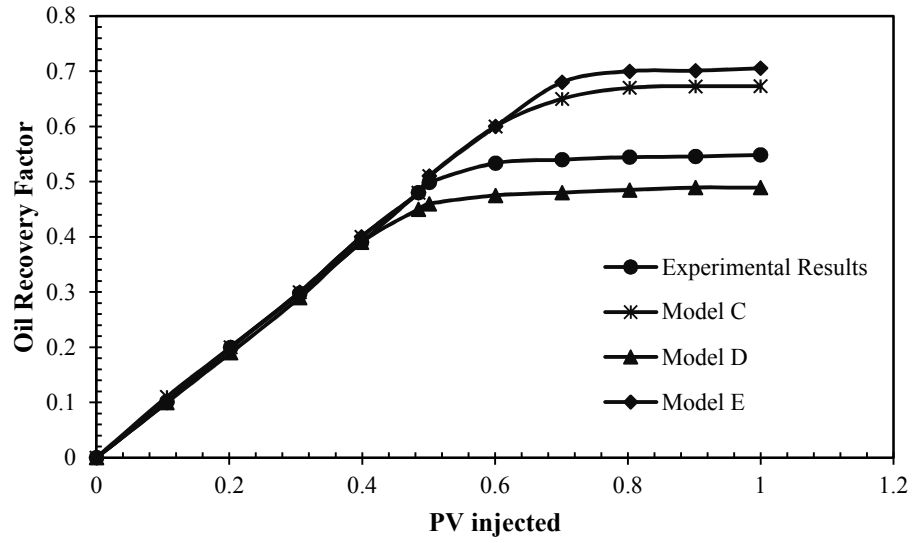
Fig.7.*Fig.7.* The oil recovery factor of models C, D and E with different pore shapes.

Fig. 8.

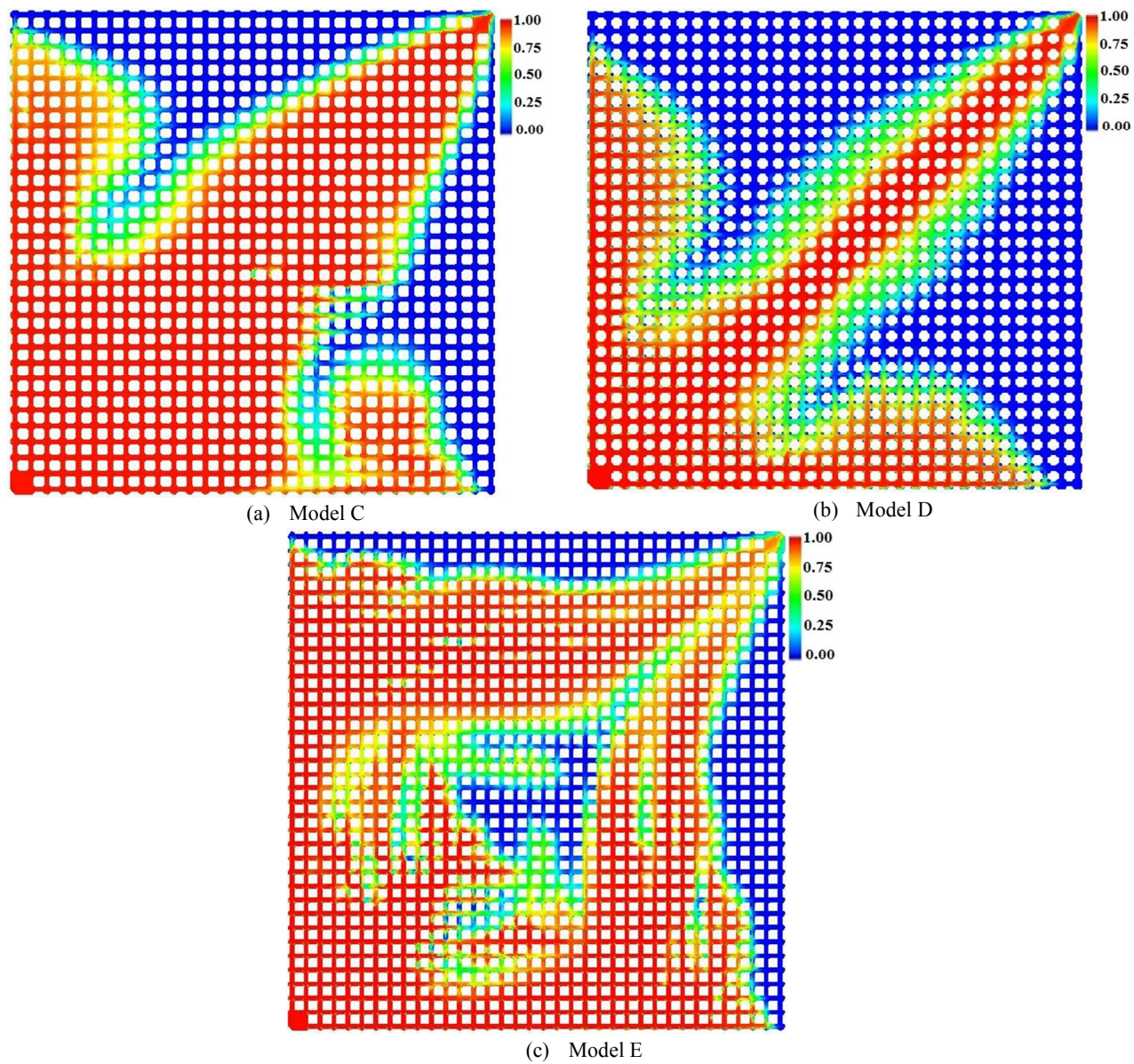


Fig. 8. The nanofluid Volume fraction contours in models C, D and E.

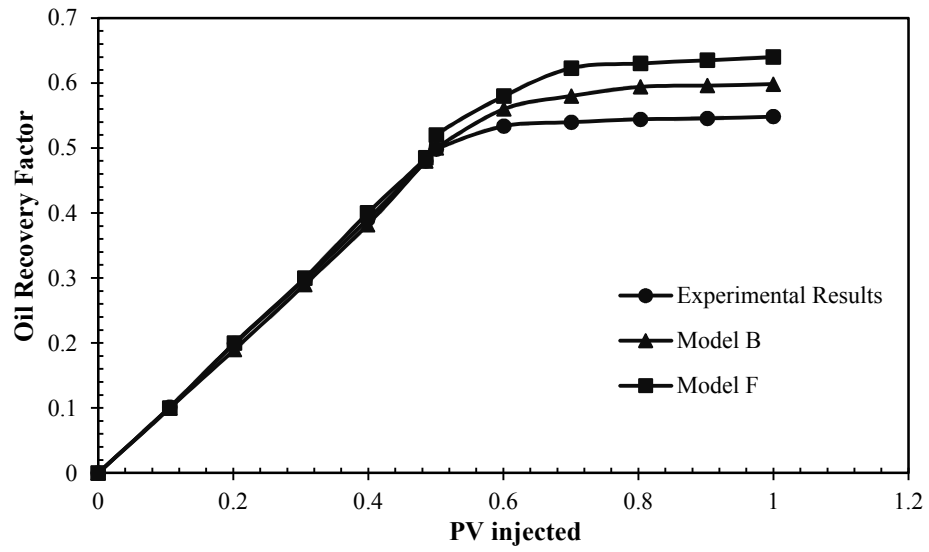
Fig. 9.*Fig. 9.* The oil recovery factor of models without throat connections.

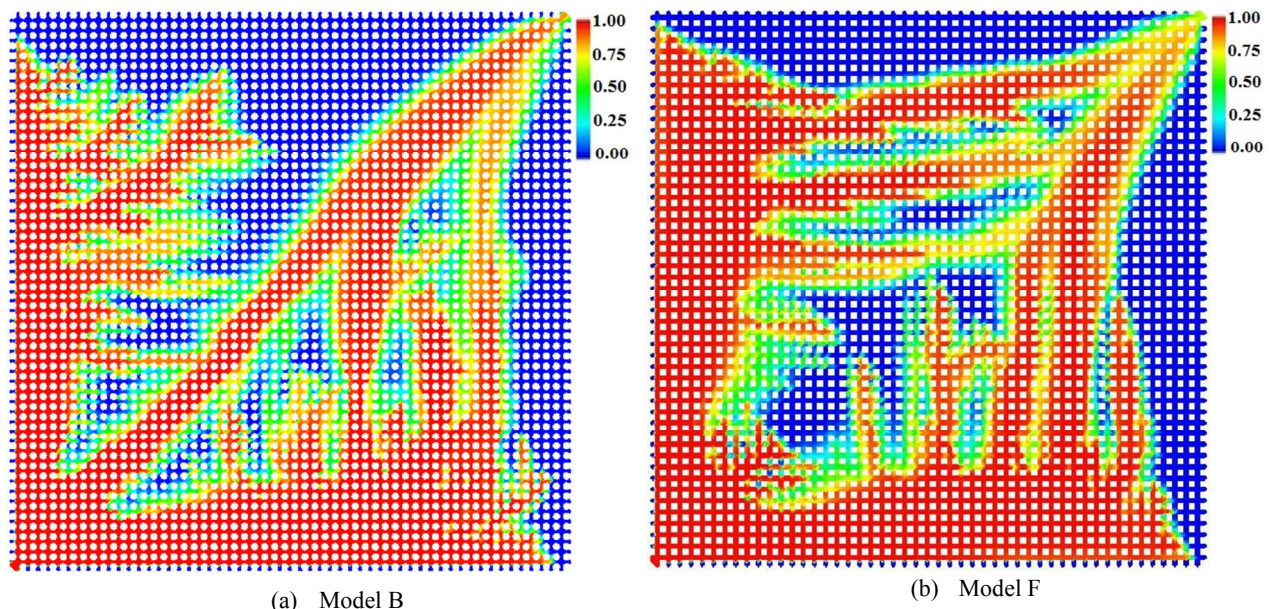
Fig. 10.**Fig. 10.** The nanofluid volume fraction contours in models B and F.

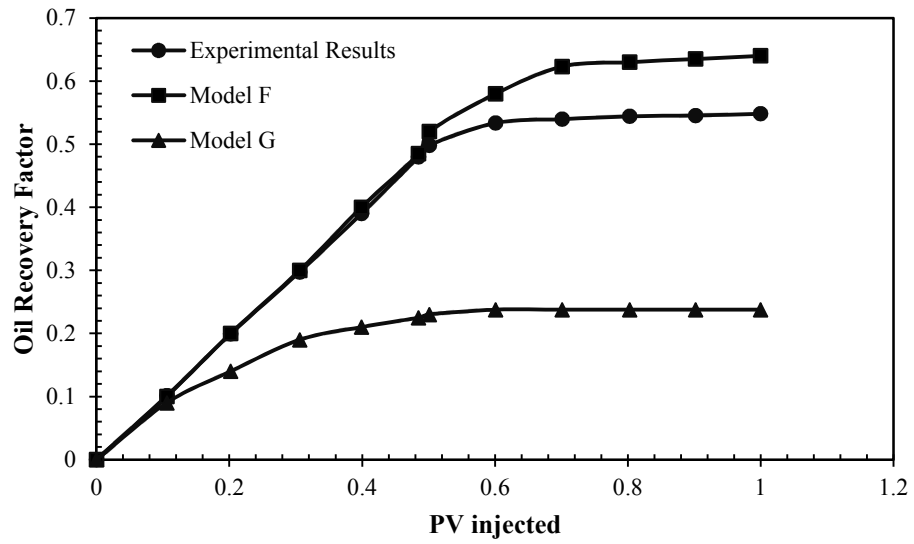
Fig. 11.*Fig. 11.* The effect of angle between fluid flow direction and pores connection on the oil recovery factor.

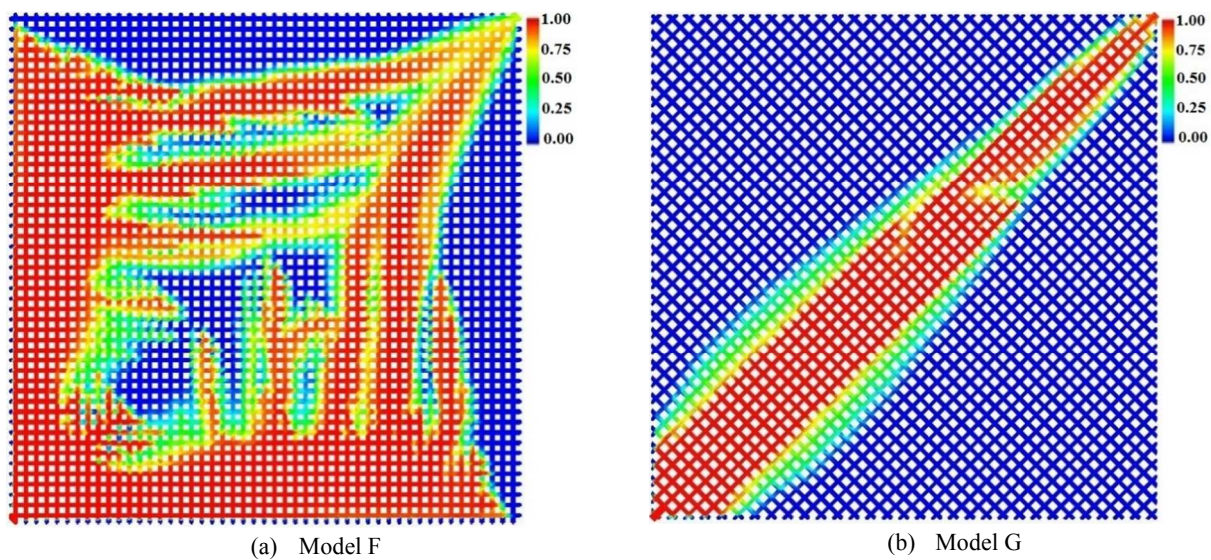
Fig. 12.

Fig. 12. The nanofluid volume fraction contours in model F and G.

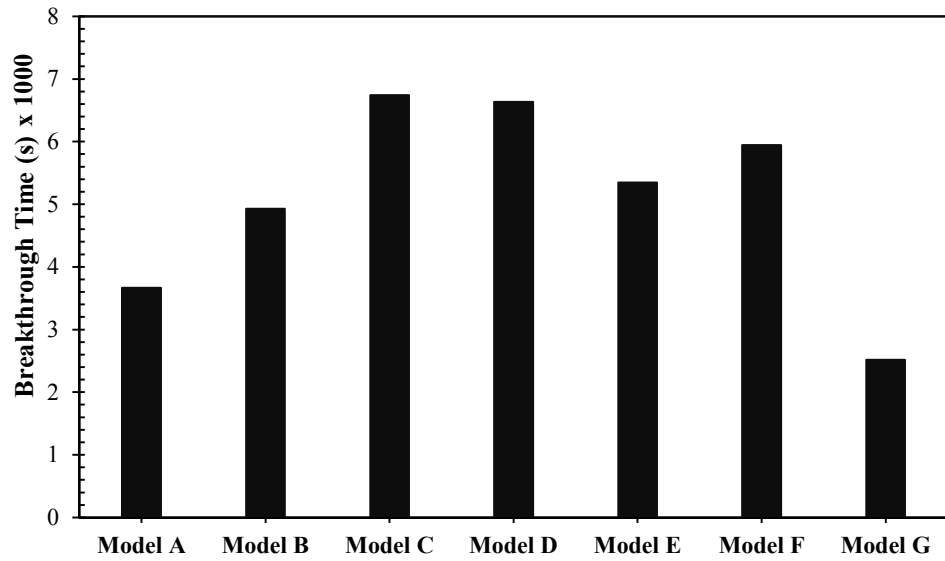
Fig. 13.*Fig. 13.* The nanofluid breakthrough time in different micromodels.

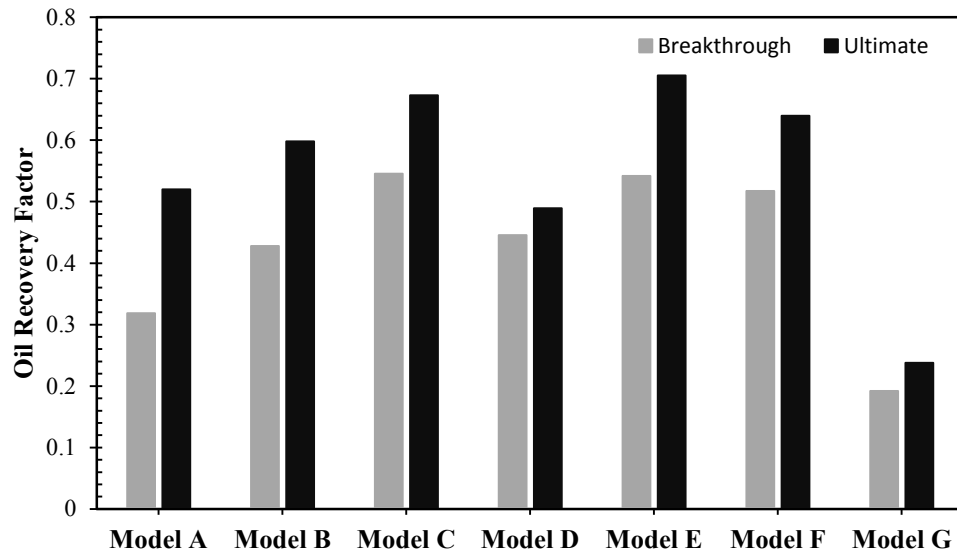
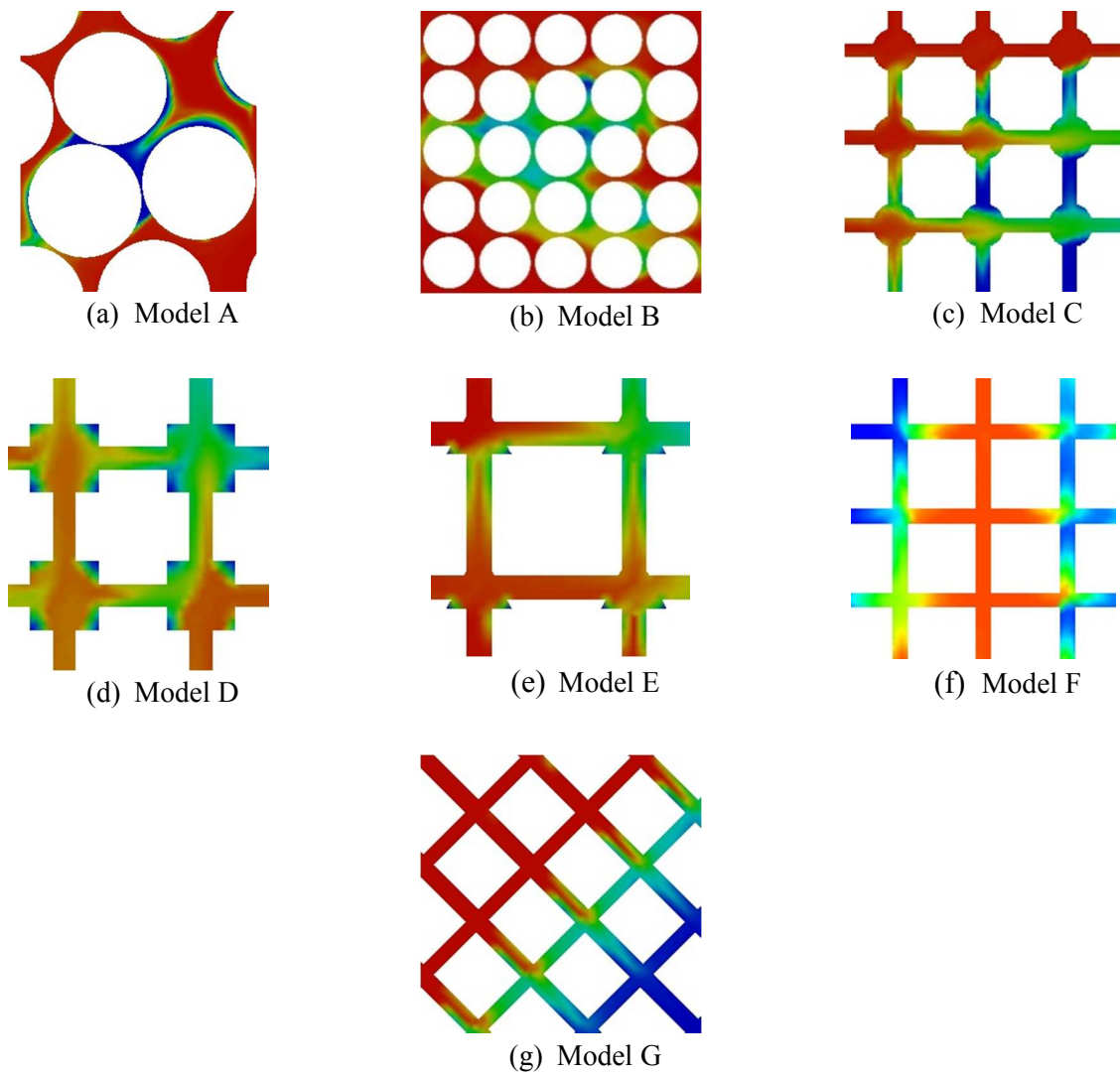
Fig.14.*Fig.14.* The oil recovery factor at breakthrough time and the ultimate oil recovery.

Fig.15.*Fig.15.* Nanofluid volume fraction contours in models A-G at the pore scale level.

List of Tables

Table 1. The physical properties of micromodels.

Table 2. The pressure drop at different grids in micromodels (A-G).

Table 3. Properties of silica nanoparticles.

Table 4. Properties of the crude oil.

Table 5. The relative error between numerical results and experimental data in models A-G.

*Table 1.**Table 1. The physical properties of micromodels.*

<i>Micromodel</i>	<i>Dimension (cm)</i>	<i>Porosity</i>	<i>Absolute Permeability (m²)</i>	<i>Coordination Number</i>
A	6×6	0.33	3.63E-07	4
B	6×6	32.44	5.65E-08	4
C	6×6	34.83	6.46E-07	4
D	6×6	35	4.92E-07	4
E	6×6	31.2	3.27E-07	4
F	6×6	32.72	1.94E-07	4
G	6×6	35	3.11E-07	4

Table 2.

Table 2. The pressure drop at different grids in micromodels (A-G).

Model	No.	Mesh Size			No. of Cells	No. of Nodes	ΔP (Pa.)	Relative Error (%)
		Inlet and Outlet	Other Edge	Face				
A	Grid 1	0.01	0.015	0.02	125469	78546	0.874	6.17
	Grid 2	0.008	0.01	0.02	251433	136449	0.931	2.89
	Grid 3	0.005	0.008	0.02	445385	212545	0.959	
B	Grid 1	0.01	0.015	0.02	276120	125469	2.794	10.48
	Grid 2	0.008	0.01	0.02	554803	343979	3.121	3.10
	Grid 3	0.005	0.008	0.02	720456	526549	3.221	
C	Grid 1	0.01	0.015	0.02	156998	96526	0.894	6.08
	Grid 2	0.008	0.01	0.02	335996	194980	0.952	1.82
	Grid 3	0.005	0.008	0.02	532642	300878	0.971	
D	Grid 1	0.01	0.015	0.02	177150	108516	0.389	4.19
	Grid 2	0.008	0.01	0.02	358378	208534	0.406	2.13
	Grid 3	0.005	0.008	0.02	528378	301084	0.414	
E	Grid 1	0.01	0.015	0.02	116139	81206	1.753	10.95
	Grid 2	0.008	0.01	0.02	289738	181371	1.969	2.45
	Grid 3	0.005	0.008	0.02	416597	253086	2.018	
F	Grid 1	0.008	0.015	0.02	151558	102456	3.851	7.71
	Grid 2	0.005	0.01	0.02	340236	216329	4.173	2.79
	Grid 3	0.005	0.008	0.02	485924	298654	4.293	
G	Grid 1	0.01	0.015	0.02	153229	87542	2.084	8.85
	Grid 2	0.008	0.01	0.02	330106	204572	2.287	3.95
	Grid 3	0.005	0.008	0.02	513189	398678	2.367	

Table 3.**Table 3. Properties of silica nanoparticles.**

<i>Particle</i>	<i>Average size (nm)</i>	<i>Specific surface (m²/g)</i>	<i>Density (kg/m³)</i>	<i>Molecular Weight (gr/mol)</i>
SiO ₂	14	200	2400	60.08

Table 4.

Table 4. Properties of the crude oil.

Viscosity (mpa.s)	Density (kg.m ⁻³)	°API @ 26 °c
870	933	19

Table 5.

Table 5. *The relative error between numerical results and experimental data in models A-G.*

Micromodel	The relative error between numerical results and experimental data (%)
A	5.17
B	9.08
C	22.72
D	10.81
E	28.64
F	16.7
G	56.65